

# Communication

## V-Band Fully Metallic Geodesic Luneburg Lens Antenna

O. Zetterstrom<sup>1</sup>, M. Petek, P. Castillo-Tapia<sup>2</sup>, Á. Palomares-Caballero<sup>3</sup>,  
N. J. G. Fonseca<sup>4</sup>, and O. Quevedo-Teruel<sup>5</sup>

**Abstract**—Antennas in emerging millimeter-wave (mm-wave) applications are often required to have low losses and produce a steerable directive beam. These properties are achievable with fully metallic geodesic Luneburg lens antennas. In this communication, we report the first experimental verification of a geodesic Luneburg lens antenna in the V-band. The designed lens antenna is fed with 13 waveguides providing beam switching capability in a 110° range. The lens is implemented in the parallel plate waveguide (PPW) technology. The antenna is manufactured in two pieces, and a tolerance analysis indicates that gaps between the pieces can cause a severe performance degradation. Based on this tolerance analysis, two measures are taken to alleviate the manufacturing tolerances for the prototype. First, electromagnetic band gap (EGB) structures are placed around the feeding waveguides. Second, the electrical contact between the two pieces is improved in critical regions. Two prototypes are manufactured, one without and one with the extra measures implemented. The measured radiation patterns of the prototype without these measures have high side lobes and low realized gain compared with the simulation. The measurements of the robust version of the prototype agree well with the simulations and demonstrate the applicability of geodesic Luneburg lens antennas for applications in the V-band.

**Index Terms**—Fully metallic antenna, geodesic lens, Luneburg lens antenna, multiple beam antenna, V-band.

### I. INTRODUCTION

Many emerging applications are intended to operate at millimeter-wave (mm-wave) frequencies, including next-generation cellular network communications [1], also integrating non-terrestrial networks [2], and radars [3], to extend the capabilities of the existing systems. Presently, the K- to W-bands are being considered due to the wide available spectrum [4]. To overcome the high propagation losses at these frequencies, the antennas are required to produce directive beams, and wide angle beam scanning is often requested. Luneburg lens antennas have been proposed to meet these requirements [5].

A Luneburg lens is a rotationally symmetric gradient index lens that when fed from the edge of the lens produces a directive beam in the diametrically opposite direction [6]. The directive beam can be steered without scan losses by moving the feeding point on the surface of the lens. Due to the gradient refractive index,

Manuscript received 18 June 2022; revised 3 November 2022; accepted 26 November 2022. Date of publication 19 December 2022; date of current version 3 February 2023. This work was supported in part by the Strategic Innovation Program Smarter Electronics System under Project High-Int 2019-02103. The work of O. Zetterstrom was supported by the European Space Agency (ESA) under Contract 4000125905/18/NL. The work of P. Castillo-Tapia, Á and O. Quevedo-Teruel was supported by the VR Project under Grant 2019-03933. (*Corresponding author: O. Zetterstrom.*)

O. Zetterstrom, P. Castillo-Tapia, and O. Quevedo-Teruel are with the Division of Electromagnetic Engineering, KTH Royal Institute of Technology, 11428 Stockholm, Sweden (e-mail: oskarz@kth.se).

M. Petek is with the Department of Electronics and Telecommunications, Politecnico di Turin, 10129 Turin, Italy.

Á. Palomares-Caballero is with the Department of Signal Theory, Telematics and Communications, University of Granada (UGR), 18071 Granada, Spain.

N. J. G. Fonseca is with the Antenna and Sub-Millimeter Waves Section, European Space Agency, 2200 AG Noordwijk, The Netherlands.

Color versions of one or more figures in this communication are available at <https://doi.org/10.1109/TAP.2022.3228690>.

Digital Object Identifier 10.1109/TAP.2022.3228690

the realization of Luneburg lenses can be challenging. 3-D Luneburg lenses have been manufactured in layers [7] or using quasi-periodic structures [8]. However, most reported 3-D Luneburg lenses require dielectric materials that introduce losses often prohibitive at mm-wave frequencies. A fully metallic 3-D Luneburg lens, based on wired media, was proposed in [9]; however, its matching to free-space is challenging, making this configuration difficult to be used as an antenna.

2-D Luneburg lens antennas are typically implemented in the parallel plate waveguide (PPW) technology [10], [11], [12], [13], [14], [15], [16], [17], [18], [19], [20], [21], [22], [23], [24]. The gradient refractive index of the lens can be mimicked with a quasi-periodic structure [14], [16], [20], PPWs with varying air gaps [13], [15], [17], or a geodesic surface [10], [11], [12], [24]. The operation of Luneburg lenses based on fully metallic quasi-periodic structures has been broadly demonstrated at the K<sub>a</sub>-band. However, as the frequency increases, the periodic inclusions become smaller and their manufacturing results in complex and costly hardware [25], [26]. The lenses based on PPWs with varying air gaps have no small details, and therefore, the manufacturing complexity of these lenses is significantly lower [13], [15], [17]. On the other hand, these lenses typically operate with the dispersive TE<sub>1</sub> PPW mode and are therefore limited in bandwidth. The PPW can be partially filled with dielectric to enable operation using the transverse electromagnetic (TEM) mode [15], at the cost of increased losses. In a geodesic lens, a fully metallic PPW is smoothly deformed in the vertical direction to mimic a refractive index [10], [11] without added losses. Since the deformed PPW is smooth (i.e., without small details), the manufacturing complexity of a geodesic lens is relatively low at mm-wave frequencies. Furthermore, since the geodesic surface is designed to equalize electrical paths, geodesic lenses are ultra-wideband.

Geodesic Luneburg [18], [21] and half-Luneburg [22] lens antennas have been reported at the K<sub>a</sub>-band. Beam-steering up to ±60° in one plane with less than 1 dB scan losses have been demonstrated [18]. To improve the crossover gain between beams when beam-steering, a geodesic near-field focused lens was proposed in [27]. The improvement in the beam crossover gain comes at a cost of reduced peak gain. In [28], a PPW is deformed to design a lens antenna based on nonrotational symmetric lenses. The feeding is mechanically moved to scan the beam continuously ±50° in one plane; however, since the lens is not rotationally symmetric, scan losses of almost 3 dB are observed.

In the present work, we demonstrate the applicability of geodesic Luneburg lens antennas in the V-band. Specifically, we design a geodesic Luneburg lens antenna operating over the band 56–62 GHz. The presented design is based on the antenna developed in [29]. This is the first time that a geodesic lens antenna is experimentally demonstrated at this high frequency, which imposes challenges in the manufacturing and assembling of the lens. We discuss the importance of using robust and cost-effective methods to improve the isolation between the feeding waveguides. The insights from this study are expected to also benefit future developments at even higher frequencies.

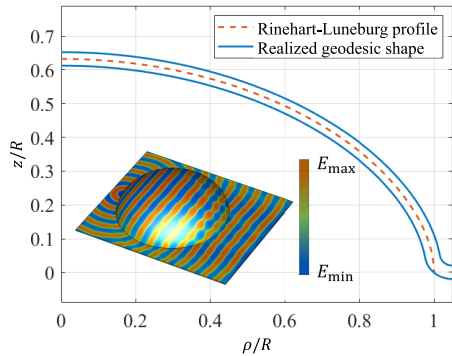


Fig. 1. Profile of a geodesic surface that mimics the operation of a Luneburg lens, known as Rinehart–Luneburg lens. The inset shows the electric field distribution in this geodesic Luneburg lens excited with a point source at the border of the lens.

The communication is outlined as follows. In Section II, the components of a geodesic Luneburg lens antenna are presented. In Section III, a tolerance analysis is provided demonstrating the need for a design that is robust to manufacturing and assembling tolerances. Corrective measures are implemented resulting in a design more tolerant to assembly gaps. In Section IV, the simulation and measurement results for the lenses without and with corrective measures are presented. A comparison of the measured response of the two antennas further validates the need for a robust implementation. Finally, the conclusions of the work are presented in Section V.

## II. GEODESIC LUNEBURG LENS ANTENNAS

The presented geodesic Luneburg lens antenna consists of a lens, feeding, and flare. In the following, we outline the design of these components.

### A. Geodesic Luneburg Lens

The rotationally symmetric gradient refractive index of the Luneburg lens is given by  $n(\rho) = \sqrt{2 - \rho^2/R^2}$ , where  $\rho$  is the radial position in the lens, and  $R$  is the radius of the lens [6]. Parallel rays impinging on this refractive index distribution are focused in a point at the surface of the lens. Since the optical path is equal for all the rays, they arrive in-phase at the focal point. In other words, the Luneburg lens has no phase aberrations.

In the 1940s, Rinehart demonstrated that the optical paths in a 2-D Luneburg lens can be mimicked with a curved surface [10] filled with a homogeneous medium (typically air). The height profile derived by Rinehart (assuming  $z = 0$  at  $\rho = R$ ) is illustrated with the red dashed line in Fig. 1. A geodesic lens is designed by rotating the Rinehart–Luneburg profile around the  $z$ -axis ( $\rho = 0$ ). The obtained surface is used as a mean surface for the two PPW conductors (illustrated with blue solid lines in Fig. 1). To avoid higher order PPW modes in the geodesic lens, the distance between the two conductors must be smaller than  $\lambda/2$ , where  $\lambda$  is the free-space wavelength at the highest operating frequency. In practice, this value is generally set around  $\lambda/4$  to provide some margin. In this work, the distance between the two conductors is 0.8 mm. A circular transition is added around  $\rho = R$  to mitigate the reflections between the lens and a surrounding planar PPW. Its design is optimized to minimize phase aberrations. The *time-domain solver* of *CST Microwave Studio* [30] is used to demonstrate the focusing property of a geodesic lens in the inset of Fig. 1. The profile in Fig. 1 is used to design a geodesic Luneburg lens with a radius of  $R = 20$  mm (i.e.,  $4\lambda$  at 60 GHz).

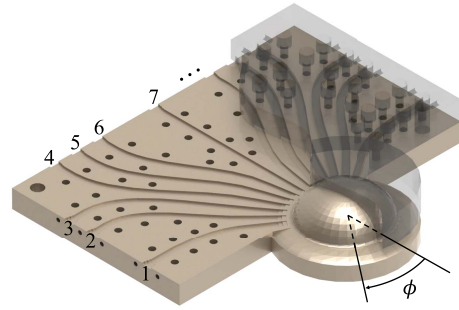


Fig. 2. Integrated lens antenna with the port numbers indicated.

### B. Feeding and Flare Design

Rectangular waveguides are used to feed the proposed lens. The waveguides are stepped to match their impedance to the impedance of the PPW lens. The stepped transitions are the same as in [29]. Due to the small spacing between the conductors of the PPW, a flare is used to mitigate the reflections at the output of the lens, providing a smooth transition to free-space. In this work, we use an exponential flare that is placed around the contour of the lens. The flare design is the same as in [29].

## III. MANUFACTURING AND ASSEMBLING CONSIDERATIONS

In this section, the integration of geodesic lens antennas in the V-band is presented. While such lenses have demonstrated excellent performance in the Ka-band using milling techniques [18], [21], a tolerance analysis indicates that manufacturing errors can significantly reduce the performance in the V-band. While part of the degradation is due to the higher operating frequency, another important aspect is the use of waveguide flanges here requiring longer feeding waveguides in place of the more compact coaxial-to-waveguide transitions used in previous works. The lens antenna design is thus adapted to be more robust to manufacturing errors. A tolerance analysis of the robust lens antenna demonstrates that the performance impairment from manufacturing and assembling errors is notably reduced.

### A. Tolerance Analysis in V-Band

The integrated lens antenna is illustrated in Fig. 2. About 13 waveguide feeds are placed along the contour of the lens, of which seven are numbered in Fig. 2, starting with the most scanned one as port 1 and with port 7 as the central one. The remaining ports are symmetric to ports 1–6. Each feed produces a directive beam at the diametrically opposite side of the lens. The feeds are mutually displaced by  $9.2^\circ$ , and thus, the antenna covers a  $110^\circ$  range in one plane. Depending on the complete antenna system implementation including electronics, these feeding ports may be used to implement beam-steering through port switching or simultaneous multiple beam operation. The waveguide feeds are extended out to the edges of a rectangular base where WR19 standard waveguides can be connected for test purposes. The feeding waveguides are designed to accommodate the flanges of the coaxial-to-waveguide transitions used in the measurements. These are significantly longer than those necessary at Ka-band [18], [21], increasing the susceptibility of the design to manufacturing errors.

The antenna is manufactured in two parts that are joined together with screws. In Fig. 2, the top part is transparent and partly hidden for illustration purposes. Screw holes for joining the two pieces are indicated in Fig. 2. It is worth noting that due to the small distance between the feeding waveguides close to the lens, more screws cannot be added in that region.

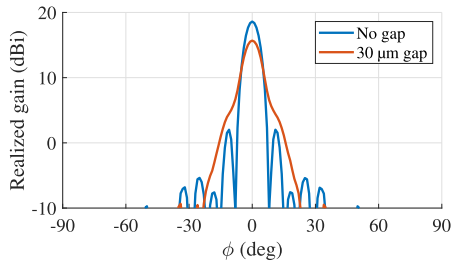


Fig. 3. Simulated realized gain at 60 GHz in the scanning plane for port 7 assuming perfect contact and a 30  $\mu\text{m}$  gap between the two pieces of the geodesic Luneburg lens.

Perfect contact between the two pieces is difficult to ensure everywhere as a result of manufacturing and assembling tolerances despite the use of high-precision milling. These errors are likely to produce randomly distributed gaps between the two metallic pieces. The mechanical design of the lens in two blocks due to the PPW configuration forces to cut the feeding waveguides through their H-plane, thus cutting through strong currents. This obviously results in localized leakage in the areas of poor contact. The effects of mechanical errors on antenna parameters are difficult to evaluate exhaustively. We provide here an assessment of the sensitivity of the design by comparing the simulated realized gain for port 7 of the lens antenna assuming perfect contact and a constant 30  $\mu\text{m}$  gap between the two pieces. Although not representative of a practical case, this constant gap is easier to implement in the full-wave model. The obtained patterns are presented in Fig. 3. We observe that the presence of the gap significantly reduces the gain and distorts the radiation pattern of the lens antenna. The significant performance degradation despite the very small gap value considered shows how critical tolerances may be at the V-band.

It is worth noting that the rectangular base needed for testing purposes can increase the unintentional gap. A transmitter or receiver based on the geodesic lens concept may not need to connect to coaxial-to-waveguide transitions, which means that the size of the rectangular base may be reduced in a practical device. However, integration of additional functionalities (e.g., filtering) and the electronics require some space, and, as a result, similar performance degradation as observed can be expected in a complete device. In Section III-B, we discuss methods to mitigate the effect of the unintentional gap. These methods are then used to design a robust version of the lens antenna.

### B. Robust V-Band Geodesic Luneburg Lens Antenna

Periodic structures can exhibit an electromagnetic band gap (EBG) that is useful for suppressing leakage in imperfect waveguide components [31]. Gap waveguides are designed to be manufactured in two pieces that are joined together with screws [31], [32]. EBG structures are placed along the two lateral sides of the waveguide to suppress the leakage that can occur if the two pieces are not in perfect electrical contact. Gap waveguides are attractive at mm-wave frequencies since small imperfections in the manufacturing can result in significant leakage as observed in Section III-A.

Glide-symmetric holey periodic structures have demonstrated similar EBG response [33], [34], [35]. These EBGs have been used to design gap waveguides at mm-waves [36]. Here, we use a 1-D glide-symmetric holey EBG structure to suppress the leakage in the lens antenna. The EBG structure and the arrangement of the holes along the lateral sides of the waveguides are illustrated in Fig. 4.

In some regions, the spacing between the waveguides is small, which must be considered in the design of the EBG structure.

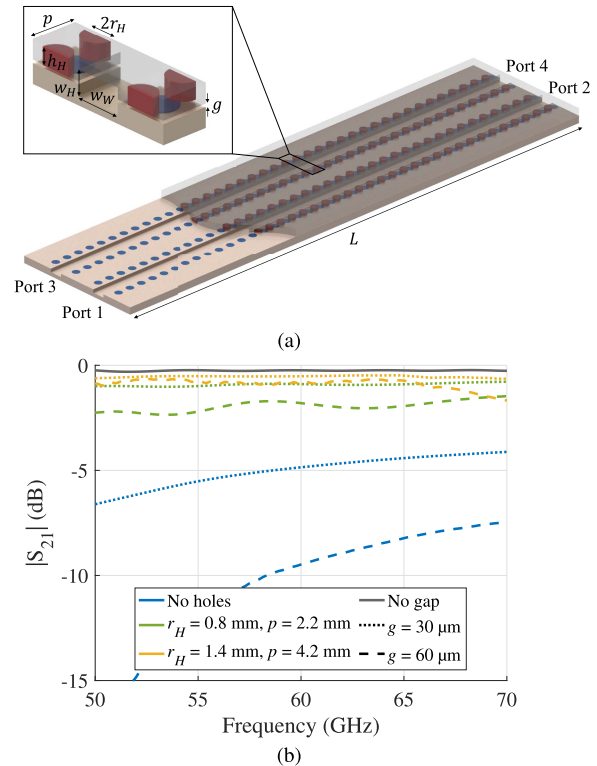


Fig. 4. (a) Simulated structure to design the EBG structure. (b) Comparison of the power transfer between ports 1 and 2 in the structure in (a) for different gaps and dimensions of the EBG structure. The remaining dimensions are:  $w_W = 3.2$  mm,  $w_H = 2.4$  mm,  $h_H = 1.4$  mm, and  $L = 200$  mm.

Fig. 4(a) illustrates the simulation setup used to design the EBG structure. The coupling between ports 1 and 2 is simulated for different parameters of the glide-symmetric structure and gaps of 30 and 60  $\mu\text{m}$ . The power transfer with glide-symmetric holes along the waveguide walls is compared with the shielded waveguide and waveguides with 30 and 60  $\mu\text{m}$  gaps and no holes. One large and one small set of holes are designed. The simulated results are presented in Fig. 4(b). The dimensions for the large holes are:  $w_W = 3.2$  mm,  $w_H = 2.4$  mm,  $p = 4.2$  mm,  $r_H = 1.4$  mm, and  $h_H = 1.4$  mm. The dimensions for the small holes are:  $w_W = 3.2$  mm,  $w_H = 2.4$  mm,  $p = 2.2$  mm,  $r_H = 0.8$  mm, and  $h_H = 1.4$  mm. The length of the structure,  $L$ , is 200 mm and it is made of aluminum in the simulations. It is observed that the holes significantly reduce the leakage from the waveguide when compared with the same configuration with no holes. The results reported also demonstrate that the leakage reduction is preserved for larger gaps, indicating the response of the EBG is tolerant to this parameter. Furthermore, we observe that the larger holes suppress the leakage more than the smaller holes.

Fig. 5 illustrates the integration of the holes in the lens antenna. Due to their larger leakage suppression, large holes are placed between the majority of the waveguides. Small holes are placed where large holes cannot be used. Furthermore, in the region nearest the lens, the waveguides are too closely spaced to place any holes. To improve the electrical contact in this region, an intentional 30  $\mu\text{m}$  air gap is implemented in the highlighted region in Fig. 5. As the screws are tightened, they will apply higher pressure in the areas without 30  $\mu\text{m}$  air gap, resulting in improved contact.

We repeat the above tolerance analysis for the robust lens antenna. Again, two scenarios are compared. First, the lens antenna is simulated with only the intentional gap (highlighted in Fig. 5). We note that the two pieces are in contact in the region without the intentional

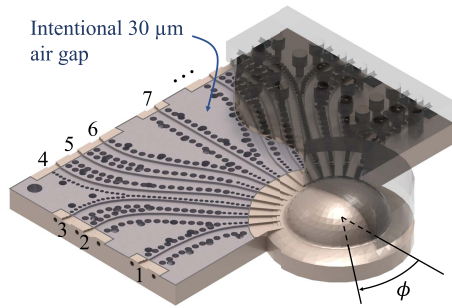


Fig. 5. Robust geodesic lens antenna with the port numbers indicated. Two sizes of EBG holes are used to suppress the leakage from the waveguides. An intentional gap is created in the region where holes are placed to improve the electrical contact in regions where the holes cannot be placed.

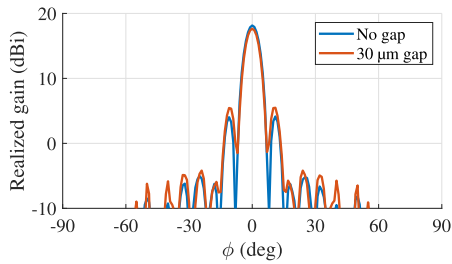


Fig. 6. Simulated realized gain at 60 GHz in the scanning plane for port 7 of the robust lens antenna assuming perfect contact and a  $30\ \mu\text{m}$  gap between the pieces.

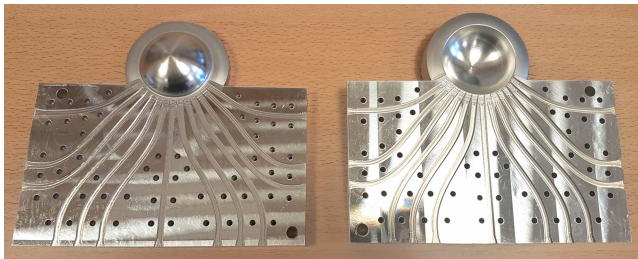


Fig. 7. Prototype of the original lens antenna.

gap. Second, the antenna is simulated with an extra  $30\ \mu\text{m}$  gap (i.e., in addition to the intentional gap). In this case, there is no contact between the pieces. The obtained patterns are presented in Fig. 6. We observe that the effect of the unwanted gap is significantly reduced in the robust antenna, compared with the original design. This comes at the expense of a slightly degraded sidelobe level, but this does preserve the design from more severe performance degradation.

#### IV. SIMULATION AND MEASUREMENT RESULTS

To further demonstrate the importance of the measures taken in the robust lens antenna, we manufacture, test, and compare the original and robust lens antennas. The manufactured prototype of the original and robust lens antennas is presented in Figs. 7 and 8(a). Fig. 8(b) presents a close-up view of the glide-symmetric EBG structure, and Fig. 8(c) shows the assembled robust lens antenna. The prototypes are manufactured with computer numerical control (CNC) milling.

The reflection coefficients of the lens antennas are evaluated using *CST* and measured using an Anritsu MS4647B VNA. The results for ports 1–7 are presented in Figs. 9 and 10 for the original and robust lens antennas, respectively. We target a reflection coefficient lower than  $-10\ \text{dB}$  in the operational band (indicated with the

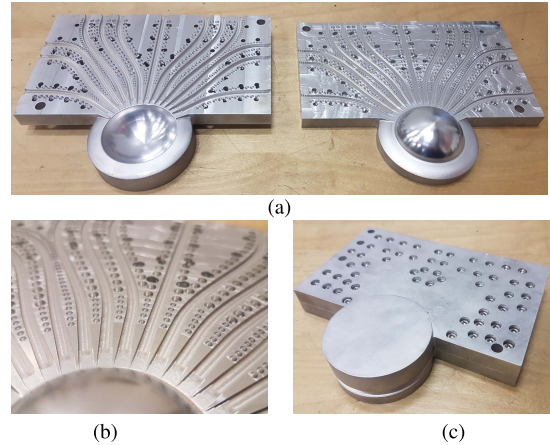


Fig. 8. (a) Prototype of the robust geodesic lens antenna. (b) Close-up view of the glide-symmetric EBG structure. (c) Assembled lens antenna.

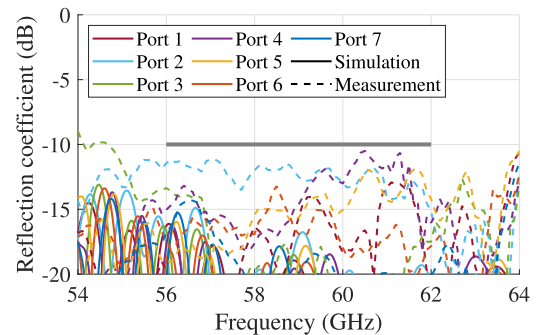


Fig. 9. Simulated and measured reflection coefficients for ports 1–7 in the original lens antenna.

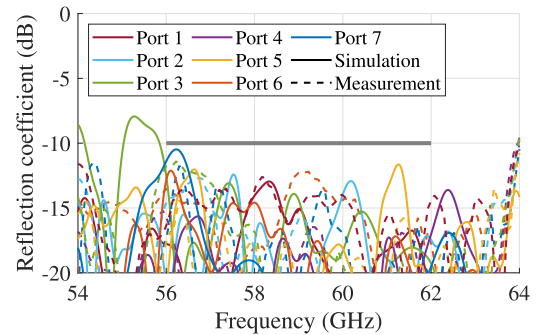


Fig. 10. Simulated and measured reflection coefficients for ports 1–7 in the robust geodesic lens antenna.

gray lines). Note that the  $30\ \mu\text{m}$  air gap (highlighted in Fig. 5) is included in the simulations for the robust lens antenna. The measured results are time-gated to remove the effect of the connecting coaxial-to-waveguide transition (i.e., the reflections in the transition are compensated for). The reflection coefficients in the operational band are below  $-10\ \text{dB}$  in simulations and measurements. A better agreement between simulations and measurements is observed with the robust design.

The simulated and measured normalized radiation patterns in the scanning plane for ports 1–7 of the original lens at 56, 58, 60, and 62 GHz are presented in Fig. 11. High sidelobe levels (SLLs) are observed in measurements. Furthermore, it is observed that the SLL is the highest at the lowest operational frequency. In Fig. 12, the simulated and measured peak realized gains for ports 1–7 are

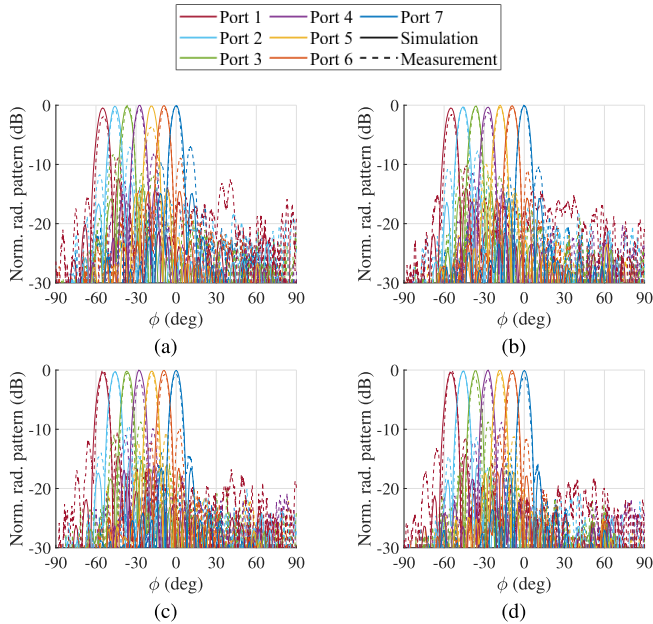


Fig. 11. Simulated and measured normalized radiation patterns in the H-plane of the original lens antenna at (a) 56, (b) 58, (c) 60, and (d) 62 GHz.

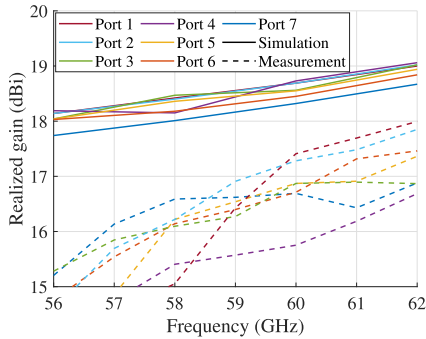


Fig. 12. Simulated and measured realized gains for ports 1–7 in the original lens antenna.

presented. The measured gain varies significantly between the ports and is roughly 1.5–4 dB lower than the simulated gain across the operational band. The discrepancies between the simulated and measured results are attributed to the manufacturing and assembling errors discussed in Section III. Due to the gap between the two pieces, leakage between the waveguides occurs, which results in increased SLL and reduced gain. We also observe that the proximity of port 1 to the edge of the rectangular base causes some of the leaked energy from port 1 to radiate at positive  $\phi$  angles. The leakage (and performance impairment) is the highest at the lowest operational frequency since the  $TE_{10}$  waveguide mode is more confined at higher frequencies.

The simulated and measured normalized radiation patterns in the scanning plane for ports 1–7 of the robust lens antenna at 56, 58, 60, and 62 GHz are presented in Fig. 13. The measured SLL is below  $-10$  dB for all the ports at all the frequencies and around  $-15$  dB for most ports and frequencies reported. In Fig. 14, the simulated and measured peak realized gains for ports 1–7 are presented. The measured gain is 1–1.5 dB lower than the corresponding simulated gain. These results are significantly improved when compared with the results of the original antenna, demonstrating the importance of the extra measures taken in the robust lens antenna. These results

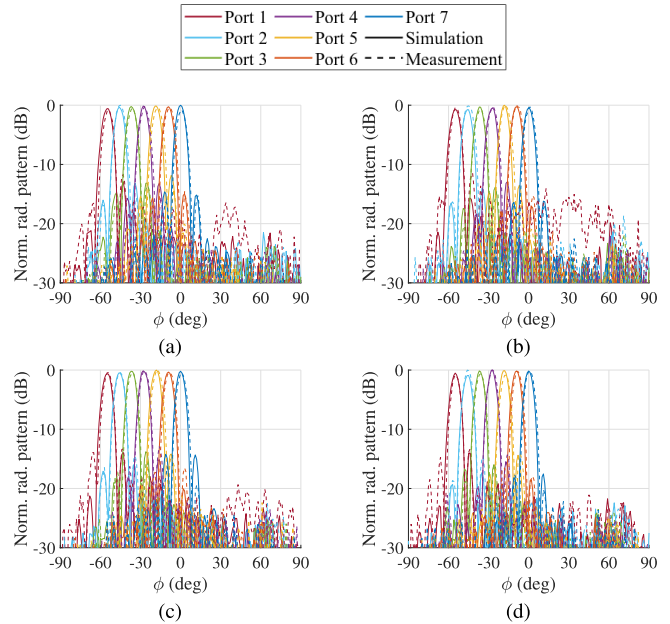


Fig. 13. Simulated and measured normalized radiation patterns for the robust geodesic lens antenna in the H-plane at (a) 56, (b) 58, (c) 60, and (d) 62 GHz.

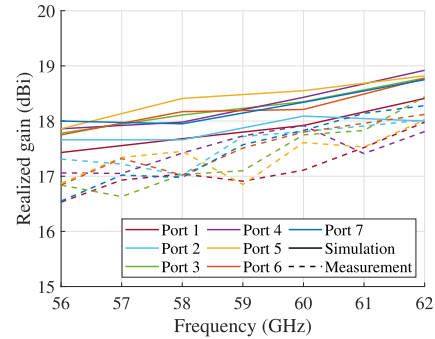


Fig. 14. Simulated and measured realized gains for ports 1–7 in the robust geodesic lens antenna.

TABLE I  
PLANAR LUNEBURG LENS ANTENNAS OPERATING ABOVE 50 GHz

Ref.	Implementation	Frequency	Rad. eff.
[37]	Compressed foam	57–65 GHz	$\approx 60\%$
[38]	Concentric dielectric cylinders	76–83 GHz	$\approx 65\%$
[39]	Drilled substrate	78–81 GHz	$\leq 60\%$
This work	Geodesic shape	56–62 GHz	$\approx 75\%$

provide valuable lessons and design guidelines for such antennas at high frequency. Table I shows comparison of the presented geodesic Luneburg lens antenna with reported planar Luneburg lens antennas operating above 50 GHz. It is observed that the geodesic Luneburg lens antenna provides the highest radiation efficiency, which makes it attractive for antenna applications in the V-band and above.

### V. CONCLUSION

In this work, we design and experimentally demonstrate a geodesic Luneburg lens antenna in the V-band. The geodesic lens, implemented in the PPW technology, is fed by 13 waveguides and terminated with a flare to mitigate the reflections at the PPW to free-space interface. The antenna can steer its directive beam in a  $\pm 55^\circ$  angular range

in the azimuth plane. The antenna is intended to be manufactured in two parts, and a tolerance analysis indicates that a gap between the two parts can severely impair the performance of the antenna. The gap results in leakage between the feeding waveguides. Therefore, two cost-effective measures are taken to increase the robustness of the antenna assembly. First, EBG structures are placed between the waveguides. Second, the electrical contact is improved in critical regions.

Two prototypes are manufactured, one without the extra measures and one with. The measured radiation patterns of the prototype without the extra measures have high SLLs and low realized gain. The measurements of the robust geodesic lens antenna are in better agreement with the simulations. The measures taken to improve the performance of the lens antenna provide valuable lessons for future developments. The designed antenna is attractive for mm-wave satellite and mobile communication, as well as radar applications.

#### REFERENCES

- [1] A. Osseiran, S. Parkvall, P. Persson, A. Zaidi, S. Magnusson, and K. Balachandran. (Apr. 2020). *5G Wireless Access: An Overview*. Accessed: May 31, 2021. [Online]. Available: <https://www.ericsson.com/en/reports-and-papers/white-papers/5g-wireless-access-an-overview>
- [2] 3GPP TR 38.811. *study on New Radio (NR) to Support Non-Terrestrial Networks, V15.0.0*. Accessed: Feb. 11, 2022. [Online]. Available: [http://www.3gpp.org/ftp/Specs/archive/38\\_series/38.811/38811-f00.zip](http://www.3gpp.org/ftp/Specs/archive/38_series/38.811/38811-f00.zip)
- [3] A. Al-Hourani et al., "Millimeter-wave integrated radar systems and techniques," in *Library in Signal Processing*, vol. 7. New York, NY, USA: Academic, 2018, pp. 317–363.
- [4] Y. Wang, J. Li, L. Huang, Y. Jing, A. Georgakopoulos, and P. Demestichas, "5G mobile: Spectrum broadening to higher-frequency bands to support high data rates," *IEEE Veh. Technol. Mag.*, vol. 9, no. 3, pp. 39–46, Sep. 2014.
- [5] O. Quevedo-Teruel, M. Ebrahimpouri, and F. Ghasemifard, "Lens antennas for 5G communications systems," *IEEE Commun. Mag.*, vol. 56, no. 7, pp. 36–41, Jul. 2018.
- [6] R. K. Luneburg and M. Herzberger, *Mathematical Theory of Optics*. Providence, RI, USA: Univ. of California Press, 1964.
- [7] G. Peeler and H. Coleman, "Microwave stepped-index Luneburg lenses," *IRE Trans. Antennas Propag.*, vol. 6, no. 2, pp. 202–207, Apr. 1958.
- [8] Y. Li, L. Ge, M. Chen, Z. Zhang, Z. Li, and J. Wang, "Multibeam 3-D-printed Luneburg lens fed by magnetoelectric dipole antennas for millimeter-wave MIMO applications," *IEEE Trans. Antennas Propag.*, vol. 67, no. 5, pp. 2923–2933, May 2019.
- [9] H. Wang, Q. Chen, O. Zetterstrom, and O. Quevedo-Teruel, "Three-dimensional broadband and isotropic double-mesh twin-wire media for meta-lenses," *Appl. Sci.*, vol. 11, no. 15, p. 7153, Aug. 2021.
- [10] R. Rinehart, "A solution of the problem of rapid scanning for radar antennae," *J. Appl. Phys.*, vol. 19, no. 9, pp. 860–862, Sep. 1948.
- [11] R. Rinehart, "A family of designs for rapid scanning radar antennas," *Proc. IRE*, vol. 40, no. 6, pp. 686–688, Jun. 1952.
- [12] K. S. Kunz, "Propagation of microwaves between a parallel pair of doubly curved conducting surfaces," *J. Appl. Phys.*, vol. 25, no. 5, pp. 642–653, May 1954.
- [13] A. S. Gutman, "Modified Luneburg lens," *J. Appl. Phys.*, vol. 25, no. 7, pp. 855–859, Aug. 1954.
- [14] R. Tanner and M. Andreasen, "A wire-grid lens antenna of wide application Part I: The wire-grid lens—concept and experimental confirmation," *IRE Trans. Antennas Propag.*, vol. 10, no. 4, pp. 408–415, May 1962.
- [15] M. Vogel, "A new kind of planar waveguide Luneburg antenna for the MM-wave region," in *Proc. 13th Eur. Microw. Conf.*, Oct. 2006, pp. 413–418.
- [16] K. Sato and H. Ujiie, "A plate Luneburg lens with the permittivity distribution controlled by hole density," *Electron. Commun. Jpn.*, vol. 85, no. 9, pp. 1–12, Apr. 2002.
- [17] H. B. Molina, J. G. Marin, and J. Hesselbarth, "Modified planar Luneburg lens millimetre-wave antenna for wide-angle beam scan having feed locations on a straight line," *IET Microw., Antennas Propag.*, vol. 11, no. 10, pp. 1462–1468, Jul. 2017.
- [18] Q. Liao, N. J. G. Fonseca, and O. Quevedo-Teruel, "Compact multibeam fully metallic geodesic Luneburg lens antenna based on non-Euclidean transformation optics," *IEEE Trans. Antennas Propag.*, vol. 66, no. 12, pp. 7383–7388, Dec. 2018.
- [19] H. Lu, Z. Liu, Y. Liu, H. Ni, and X. Lv, "Compact air-filled Luneburg lens antennas based on almost-parallel plate waveguide loaded with equal-sized metallic posts," *IEEE Trans. Antennas Propag.*, vol. 67, no. 11, pp. 6829–6838, Nov. 2019.
- [20] F. Fan, M. Cai, J. Zhang, Z. Yan, and J. Wu, "Wideband low-profile Luneburg lens based on a glide-symmetric metasurface," *IEEE Access*, vol. 8, pp. 85698–85705, 2020.
- [21] N. J. G. Fonseca, Q. Liao, and O. Quevedo-Teruel, "Equivalent planar lens ray-tracing model to design modulated geodesic lenses using non-Euclidean transformation optics," *IEEE Trans. Antennas Propag.*, vol. 68, no. 5, pp. 3410–3422, May 2020.
- [22] N. J. G. Fonseca, Q. Liao, and O. Quevedo-Teruel, "Compact parallel-plate waveguide half-Luneburg geodesic lens in the Ka-band," *IET Microw., Antennas Propag.*, vol. 15, no. 2, pp. 123–130, Feb. 2021.
- [23] N. J. G. Fonseca, "The water drop lens: Revisiting the past to shape the future," *EurAAP Rev. Electromagn.*, vol. 1, no. 1, pp. 1–4, Jan. 2022.
- [24] O. Quevedo-Teruel et al., "Geodesic lens antennas for 5G and beyond," *IEEE Commun. Mag.*, vol. 60, no. 1, pp. 40–45, Jan. 2022.
- [25] D. Gonzalez-Ovejero, C. Jung-Kubiak, M. Alonso-delPino, T. Reck, and G. Chattopadhyay, "Design, fabrication and testing of a modulated metasurface antenna at 300 GHz," in *Proc. 11th Eur. Conf. Antennas Propag. (EuCAP)*, Mar. 2017, pp. 3416–3418.
- [26] D. González-Ovejero, N. Chahat, R. Sauleau, G. Chattopadhyay, S. Maci, and M. Ettore, "Additive manufactured metal-only modulated metasurface antennas," *IEEE Trans. Antennas Propag.*, vol. 66, no. 11, pp. 6106–6114, Nov. 2018.
- [27] O. Orgeira, G. Leon, N. J. G. Fonseca, P. Mongelos, and O. Quevedo-Teruel, "Near-field focusing multibeam geodesic lens antenna for stable aggregate gain in far-field," *IEEE Trans. Antennas Propag.*, vol. 70, no. 5, pp. 3320–3328, May 2022.
- [28] T. Strober, S. Tubau, E. Girard, H. Legay, G. Goussetis, and M. Ettore, "Shaped parallel-plate lens for mechanical wide-angle beam steering," *IEEE Trans. Antennas Propag.*, vol. 69, no. 12, pp. 8158–8169, Dec. 2021.
- [29] M. Petek, O. Zetterstrom, E. Pucci, N. J. G. Fonseca, and O. Quevedo-Teruel, "Fully-metallic Rinehart-Luneburg lens at 60 GHz," in *Proc. 14th Eur. Conf. Antennas Propag. (EuCAP)*, 2020, pp. 1–5.
- [30] *CST Microwave Studio*. Accessed: Feb. 14, 2022. [Online]. Available: <http://www.cst.com/>
- [31] P.-S. Kildal, E. Alfonso, A. Valero-Nogueira, and E. Rajo-Iglesias, "Local metamaterial-based waveguides in gaps between parallel metal plates," *IEEE Antennas Wireless Propag. Lett.*, vol. 8, pp. 84–87, 2008.
- [32] E. Rajo-Iglesias, M. Ferrando-Rocher, and A. U. Zaman, "Gap waveguide technology for millimeter-wave antenna systems," *IEEE Commun. Mag.*, vol. 56, no. 7, pp. 14–20, Jul. 2018.
- [33] M. Ebrahimpouri, O. Quevedo-Teruel, and E. Rajo-Iglesias, "Design guidelines for gap waveguide technology based on glide-symmetric holey structures," *IEEE Microw. Wireless Compon. Lett.*, vol. 27, no. 6, pp. 542–544, Jun. 2017.
- [34] Q. Chen, F. Mesa, X. Yin, and O. Quevedo-Teruel, "Accurate characterization and design guidelines of glide-symmetric holey EBG," *IEEE Trans. Microw. Theory Techn.*, vol. 68, no. 12, pp. 4984–4994, Dec. 2020.
- [35] O. Quevedo-Teruel, Q. Chen, F. Mesa, N. J. G. Fonseca, and G. Valerio, "On the benefits of glide symmetries for microwave devices," *IEEE J. Microw.*, vol. 1, no. 1, pp. 457–469, Jan. 2021.
- [36] M. Ebrahimpouri, E. Rajo-Iglesias, Z. Sipus, and O. Quevedo-Teruel, "Cost-effective gap waveguide technology based on glide-symmetric holey EBG structures," *IEEE Trans. Microw. Theory Techn.*, vol. 66, no. 2, pp. 927–934, Feb. 2018.
- [37] J. Bor, O. Lafond, H. Merlet, P. Le Bars, and M. Himdi, "Foam based Luneburg lens antenna at 60 GHz," *Prog. Electromagn. Res. Lett.*, vol. 44, pp. 1–7, 2013.
- [38] M. K. Saleem, H. Vettikaladi, M. A. S. Alkanhal, and M. Himdi, "Lens antenna for wide angle beam scanning at 79 GHz for automotive short range radar applications," *IEEE Trans. Antennas Propag.*, vol. 65, no. 4, pp. 2041–2046, Apr. 2017.
- [39] A. B. Numan, J.-F. Frigon, and J.-J. Laurin, "Printed W-band multibeam antenna with Luneburg lens-based beamforming network," *IEEE Trans. Antennas Propag.*, vol. 66, no. 10, pp. 5614–5619, Oct. 2018.